







# A Broad HCO<sup>+</sup> Absorption Line Associated with the Circumnuclear Torus of NGC 1052

Satoko Sawada-Satoh<sup>1</sup> , Do-Young Byun<sup>2,3</sup> , Sang-Sung Lee<sup>2,3</sup> , Se-Jin Oh<sup>2</sup>, Duk-Gyoo Roh<sup>2</sup>, Seiji Kamenno<sup>4,5</sup> ,  
Jae-Hwan Yeom<sup>2</sup>, Dong-Kyu Jung<sup>2</sup>, Chungsik Oh<sup>2</sup>, Hyo-Ryoung Kim<sup>2</sup>, and Ju-Yeon Hwang<sup>2,6</sup>

<sup>1</sup> Graduate School of Science and Engineering, Kagoshima University, 1-21-35 Korimoto, Kagoshima 890-0065, Japan; [swdsth@gmail.com](mailto:swdsth@gmail.com)

<sup>2</sup> Korea Astronomy and Space Science Institute, 776 Daedeok-daero, Yuseong, Daejeon 34055, Republic of Korea

<sup>3</sup> University of Science and Technology, 217 Gajeong-ro, Yuseong-gu, Daejeon 34113, Republic of Korea

<sup>4</sup> Joint ALMA Observatory, Alonso de Cordova 3107 Vitacura, Santiago 763 0355, Chile

<sup>5</sup> National Astronomical Observatory of Japan, 2-21-1 Osawa, Mitaka, Tokyo 181-8588, Japan

<sup>6</sup> SET system, 16-3 Gangnam-daero 8-gil, Seocho-gu, Seoul 06787, Republic of Korea

Received 2018 November 1; revised 2019 February 3; accepted 2019 February 3; published 2019 February 19

## Abstract

We present the first subparsec-scale maps of HCO<sup>+</sup>  $J = 1-0$  absorption in the circumnuclear region of the nearby radio galaxy NGC 1052. Our  $\lambda 3$  mm very-long-baseline-interferometry (VLBI) observations with the Korean VLBI Network have spatially resolved the broad HCO<sup>+</sup> absorption at a velocity range of 1350–1850 km s<sup>-1</sup> against a double-sided nuclear jet, and have revealed that the HCO<sup>+</sup> absorption is concentrated on the receding jet and the nuclear components. The distribution of the HCO<sup>+</sup> absorbing gas strongly supports the circumnuclear torus surrounding the supermassive black hole. From the estimations of the column density and the volume density of molecular hydrogen, the size of the molecular gas region in the torus is at least 1 pc. The broad spectral profile of HCO<sup>+</sup> is likely to be a blend of multiple gas clumps with various velocities. The HCO<sup>+</sup> absorption of NGC 1052 could trace complex kinematics in the vicinity of the active galactic nucleus, such as inflow, outflow, turbulence, and so on.

*Key words:* galaxies: active – galaxies: individual (NGC 1052) – galaxies: nuclei – quasars: absorption lines

## 1. Introduction

NGC 1052 is a nearby radio galaxy with a systemic velocity ( $V_{\text{sys}} = cz$ ) of 1507 km s<sup>-1</sup> (Jensen et al. 2003). It exhibits a nearly symmetric double-sided radio jet from subparsec scales up to kiloparsecs (e.g., Jones et al. 1984; Wrobel 1984; Kellermann et al. 1998), showing outward motions with an apparent velocity of 0.26c (Vermeulen et al. 2003). Past very-long-baseline-interferometry (VLBI) studies have shown that the nuclear structure consists of the eastern approaching and the western receding jets at an inclination angle of  $\geq 57^\circ$  from the line of sight (e.g., Kellermann et al. 1999; Kamenno et al. 2001; Kadler et al. 2004b). Atomic and molecular lines are found toward the center of NGC 1052 in emission (H<sub>2</sub>O megamaser for Braatz et al. 1994) and in absorption (HI for van Gorkom et al. 1986; OH for Omar et al. 2002; HCO<sup>+</sup>; HCN and CO for Liszt & Lucas 2004) at the radio band.

NGC 1052 hosts a well-studied circumnuclear torus surrounding its central engine. The presence of a parsec-scale dense plasma torus has been proposed based on the measurements of free–free absorption in the innermost region of the radio jet obtained by the multi-frequency VLBI observations (Kamenno et al. 2001, 2003; Vermeulen et al. 2003; Kadler et al. 2004b). The torus is geometrically thick, obscuring 0.1 pc and 0.7 pc of the eastern and western jets, respectively. The electron column density toward the free–free absorber is estimated to be  $\sim 10^{23}$  cm<sup>-2</sup>, which is consistent with atomic hydrogen column density of  $10^{22}$ – $10^{24}$  cm<sup>-2</sup> derived from various past X-ray observations (Guainazzi & Antonelli 1999; Weaver et al. 1999; Kadler et al. 2004a). Kamenno et al. (2005) have proposed a torus model with several phase layers: a hot plasma layer at the inner surface, a warm molecular gas layer where the H<sub>2</sub>O maser arises, and a cooler molecular layer. Several spectral VLBI observations have revealed that gases of H<sub>2</sub>O megamaser emission, OH absorption, and HCN

absorption are located where the free–free absorption is large due to the torus, which supports the torus model with several layers (Sawada-Satoh et al. 2008, 2016; Impellizzeri et al. 2008). The spectra of the H<sub>2</sub>O megamaser, OH absorption, and HCN absorption are all redshifted with respect to  $V_{\text{sys}}$ , which has been explained as being due to ongoing material infalling onto the supermassive black hole (Sawada-Satoh et al. 2008, 2016; Impellizzeri et al. 2008). These circumnuclear structures make NGC 1052 an ideal laboratory to study subparsec-scale molecular chemistry and its relation to the active galactic nucleus (AGN)-related physical and chemical process.

HCO<sup>+</sup> and HCN are both known as good dense molecular gas tracers in galaxies because of their large dipole moment and abundance. The IRAM Plateau de Bure Interferometer (PdBI) observations have discovered HCO<sup>+</sup>(1–0) absorption against NGC 1052 (Liszt & Lucas 2004). The derived spectral profile of the HCO<sup>+</sup> absorption was broad, extending from 1400 to 1900 km s<sup>-1</sup> in velocity, and was not resolved into narrow absorption features. The peak velocity of the HCO<sup>+</sup> absorption was  $\sim 1650$  km s<sup>-1</sup>, which was  $\sim 150$  km s<sup>-1</sup> redshifted from  $V_{\text{sys}}$ . It was close to the peak velocities of HCN absorption (Liszt & Lucas 2004) and H<sub>2</sub>O maser emission (Braatz et al. 1994). To confirm the broad HCO<sup>+</sup> absorption traces in the circumnuclear region of NGC 1052, one milliarcsecond (mas) angular resolution achieved by VLBI is essential. The VLBI map of molecular absorption line against the parsec-scale synchrotron radio source offers a unique scientific opportunity in direct detection of thermal molecular gas on parsec- and subparsec scales (e.g., Sawada-Satoh et al. 2016).

We have observed the high dense gas tracer HCO<sup>+</sup> transition toward the center of NGC 1052 with the Korean VLBI Network (KVN). Here we show the first detection and the maps of the subparsec-scale HCO<sup>+</sup>(1–0) absorption in the circumnuclear region of NGC 1052. One mas corresponds to 0.095 pc in the galaxy.

## 2. Observations and Data Reduction

KVN observations of NGC 1052 were carried out from 2017 June 17 UT 21:00 to June 18 UT 06:00, for a total on-source time of 7.5 hr. To improve the sensitivity for the  $\lambda 3$  mm  $\text{HCO}^+(1-0)$  absorption line observation, simultaneous dual-frequency observation was conducted at  $\lambda 1.3$  cm and  $\lambda 3$  mm bands using the KVN multi-frequency receiving system (Han et al. 2008, 2013; Oh et al. 2011). To cover the broad  $\text{HCO}^+(1-0)$  absorption feature ( $\sim 400$  km s $^{-1}$ ), the data were recorded at each station with the Mark6 system at a sampling rate of 8 Gbps ( $512$  MHz  $\times$  4 IFs  $\times$  2 bit quantization) in dual circular polarization.

Two of four intermediate frequency channels (IFs) were assigned to left-hand circular polarization (LHCP) and right-hand circular polarization (RHCP) at  $\lambda 3$  mm for the target frequency band. The other two IFs were fixed to LHCP and RHCP at  $\lambda 1.3$  cm for the phase referencing. The velocity coverage of one IF at  $\lambda 3$  mm was  $\sim 1600$  km s $^{-1}$ . For phase and bandpass calibration, 3C 84 and NRAO 150 were also observed every hour.

The data were correlated with the DiFX software correlator (Deller et al. 2007) at the Korea-Japan Correlation Center (Yeom et al. 2009; Lee et al. 2015b). The visibility amplitude decrement due to the digital quantization loss was corrected by applying a correction factor of 1.1 (Lee et al. 2015a). Post-correlation processing was done using NRAO AIPS software (Greisen 2003). A priori amplitude calibration was applied using measurements of the opacity-corrected system temperature with the chopper-wheel method (e.g., Ulich & Haas 1976) and gain curve depending on the elevation. Complex bandpass characteristics at each station were solved using data of 3C 84 and NRAO 150.

To calibrate rapid atmospheric phase fluctuations at  $\lambda 3$  mm, we analyzed these data using the frequency phase transfer (FPT) method, in which the phase solutions of the low-frequency band ( $\lambda 1.3$  cm) are transferred to the high-frequency band ( $\lambda 3$  mm) by scaling by their frequency ratio (Middelberg et al. 2005; Rioja & Dodson 2011). Applying FPT, the rms phase fluctuation was reduced by  $\sim 40\%$  for all of three baselines. Doppler velocity corrections were made by running the AIPS tasks SETJY and CVEL. The continuum was subtracted with the AIPS task UVLSF by performing a polynomial fit to line-free channels in the visibility domain. We identified channels with a velocity lower than  $1400$  km s $^{-1}$  and higher than  $1900$  km s $^{-1}$  as the line-free channels. The parallel-hand data were averaged into the total intensity data. We corrected the visibility phase using self-calibration with the averaged line-free channels, and applied the solutions of the self-calibration in the absorption line channels. The continuum map was formed from the averaged line-free channels using the hybrid imaging with CLEAN and self-calibration. The image cube was generated with a channel width of 8 MHz. The optical depth image cube was yielded from the continuum map and the image cube, and averaged every 32 MHz. We blanked image pixels with intensities below  $18$  mJy beam $^{-1}$  ( $<6\sigma$ ) in the continuum map, because the signal-to-noise ratio in optical depth is poor where the continuum emission is weak. Maps were produced with natural weighting, and the resulting FWHM of the synthesized beam is  $1.60 \times 0.87$  mas ( $0.152 \times 0.082$  pc in NGC 1052).

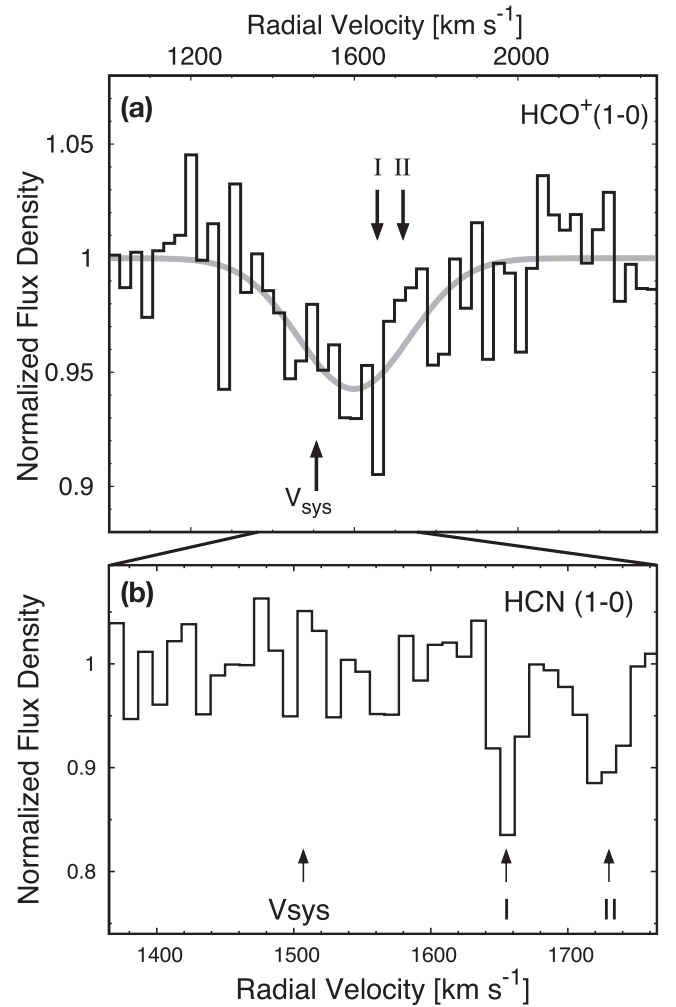


**Figure 1.** (a) Cross power spectrum of  $\text{HCO}^+(1-0)$  absorption lines integrated over the whole on-source time of NGC 1052 obtained with the KVN, represented with the black solid line. The velocity resolution is  $26.9$  km s $^{-1}$ , and the rms noise in the normalized flux density is  $0.02$ . The gray solid line gives a Gaussian fit to the absorption profile. The labels I and II represent the narrow HCN absorption features at  $1656$  and  $1719$  km s $^{-1}$ , detected with the past KVN observation (Sawada-Satoh et al. 2016). (b) Spectral profile of HCN ( $1-0$ ) absorption of NGC 1052 obtained with the KVN in 2015. The velocity resolution is  $10.5$  km s $^{-1}$ . This panel is exactly the same as Figure 1 in Sawada-Satoh et al. (2016).

## 3. Results

Figure 1(a) shows the vector-averaged cross power spectrum of  $\text{HCO}^+(1-0)$  absorption of NGC 1052 integrated over the whole on-source time with the KVN. The frequency resolution is 8 MHz, which corresponds to  $26.9$  km s $^{-1}$  in velocity resolution ( $\Delta\nu$ ). All the spectral channels are normalized to the continuum level. Broad  $\text{HCO}^+(1-0)$  absorption is detected in the velocity range from  $1350$  to  $1850$  km s $^{-1}$ . The absorption profile could be slightly asymmetrical with the blueshifted part having more extended wing than the redshifted part, and the peak absorption channel is at velocity of  $1658$  km s $^{-1}$ . The peak channel is close in velocity to the narrow HCN absorption features I at  $1656$  km s $^{-1}$ , reported in Sawada-Satoh et al. (2016; Figure 1(b)). The  $\text{HCO}^+$  spectral profile, including a redshifted peak and a blueshifted wing, and their velocities are similar to those of the absorption profile from the PdBI data (Liszt & Lucas 2004). However, the peak absorption channel at  $1658$  km s $^{-1}$  has a depth of  $-9.5\%$  of the continuum level,

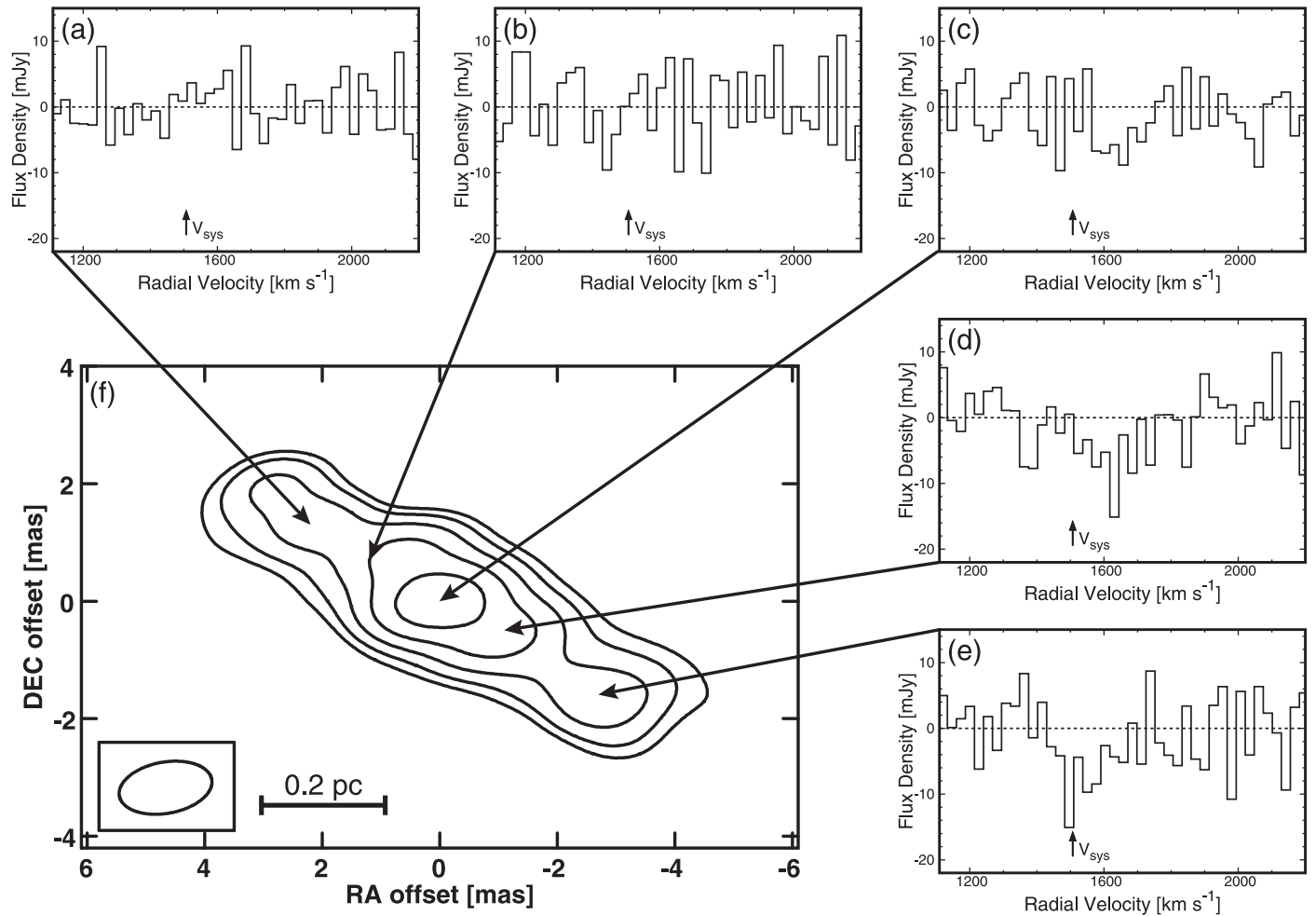


**Figure 2.** (a)–(e) Spectra of  $\text{HCO}^+(1-0)$  absorption at different locations as marked in the arrows. The velocity resolution is  $26.9 \text{ km s}^{-1}$ . Zero flux density corresponds to the continuum level for each location. (f) Continuum image of the nuclear region in NGC 1052 at  $\lambda 3 \text{ mm}$ . The contour starts at the  $3\sigma$  level, increasing by a factor of 2, where  $\sigma = 3 \text{ mJy beam}^{-1}$ . The peak intensity of the brightest component is  $244 \text{ mJy beam}^{-1}$ . The synthesized beam size is shown at the lower-left corner.

which is deeper than that of the PdBI ( $-3\%$ ). The peak absorption depth results in the peak optical depth ( $\tau_p$ ) of  $0.10 \pm 0.02$ .

To give a rough estimation of the width and the maximum depth, we attempted a single Gaussian fitting to the spectral profile, while it is rather asymmetrical. We obtained the best-fit model profile with the full widths at half depth in velocity of  $272 \pm 50 \text{ km s}^{-1}$ , and the maximum depth of  $-0.06 \pm 0.01$  at the centroid velocity of  $1599 \pm 25 \text{ km s}^{-1}$ . The reduced chi square is 1.04, and it is not further improved even if we give multiple-Gaussian fitting.

The broad  $\text{HCO}^+$  absorption is spatially resolved by the VLBI imaging. In Figure 2, we present a continuum image of the nuclear region in NGC 1052 at  $\lambda 3 \text{ mm}$  and  $\text{HCO}^+(1-0)$  absorption spectra in various regions against the background continuum emission of NGC 1052. The  $\text{HCO}^+(1-0)$  absorption spectra were extracted from the image cube using the AIPS task ISPEC integrating over the region of  $1.4 \times 1.4 \text{ mas}$  at different spatial positions. The typical  $1\sigma$  level is  $5 \text{ mJy}$  in  $8 \text{ MHz}$  ( $26.9 \text{ km s}^{-1}$ ) channel. Figures 2(a) and (b) indicate that no significant absorption feature is seen against the eastern approaching jet, while a weak absorption feature is tentatively detected on the central nuclear component at velocity of  $\sim 1650 \text{ km s}^{-1}$  as shown in Figure 2(c). Figures 2(d) and (e)

show that the absorption depth reaches  $3\sigma$  level on the western receding jet.

The  $\lambda 3 \text{ mm}$  continuum image reveals a symmetric double-sided jet structure that consists of a bright central component and two elongated eastern and western jets (Figure 2(f)). The jet structure is extended up to  $\sim 0.7 \text{ pc}$ . The flux densities of the central component within  $1.6 \text{ mas}$  (the major axis of the synthesized beam), the eastern jet, and the western jet are determined to be  $414$ ,  $92$ , and  $93 \text{ mJy}$ , by summing the CLEAN components. The continuum image is consistent with the previous KVN map at  $89 \text{ GHz}$  taken in 2015 (Sawada-Satoh et al. 2016).

$\text{HCO}^+$  optical depth channel maps superimposed on the  $\lambda 3 \text{ mm}$  continuum image are shown in Figure 3. Distribution of  $\text{HCO}^+$  optical depth on the double-sided jet structure shows that high opacities are localized on the western receding jet side, where the parsec-scale torus obscures. Such a localization of the high opacity on the receding jet side is also seen in the opacity distributions of OH (Impellizzeri et al. 2008) and HCN (Sawada-Satoh et al. 2016) of this galaxy.

#### 4. Discussions

From our KVN observations, the  $\text{HCO}^+$  opacity of  $\sim 0.4$  is derived in the nuclear region of NGC 1052 with the subparsec

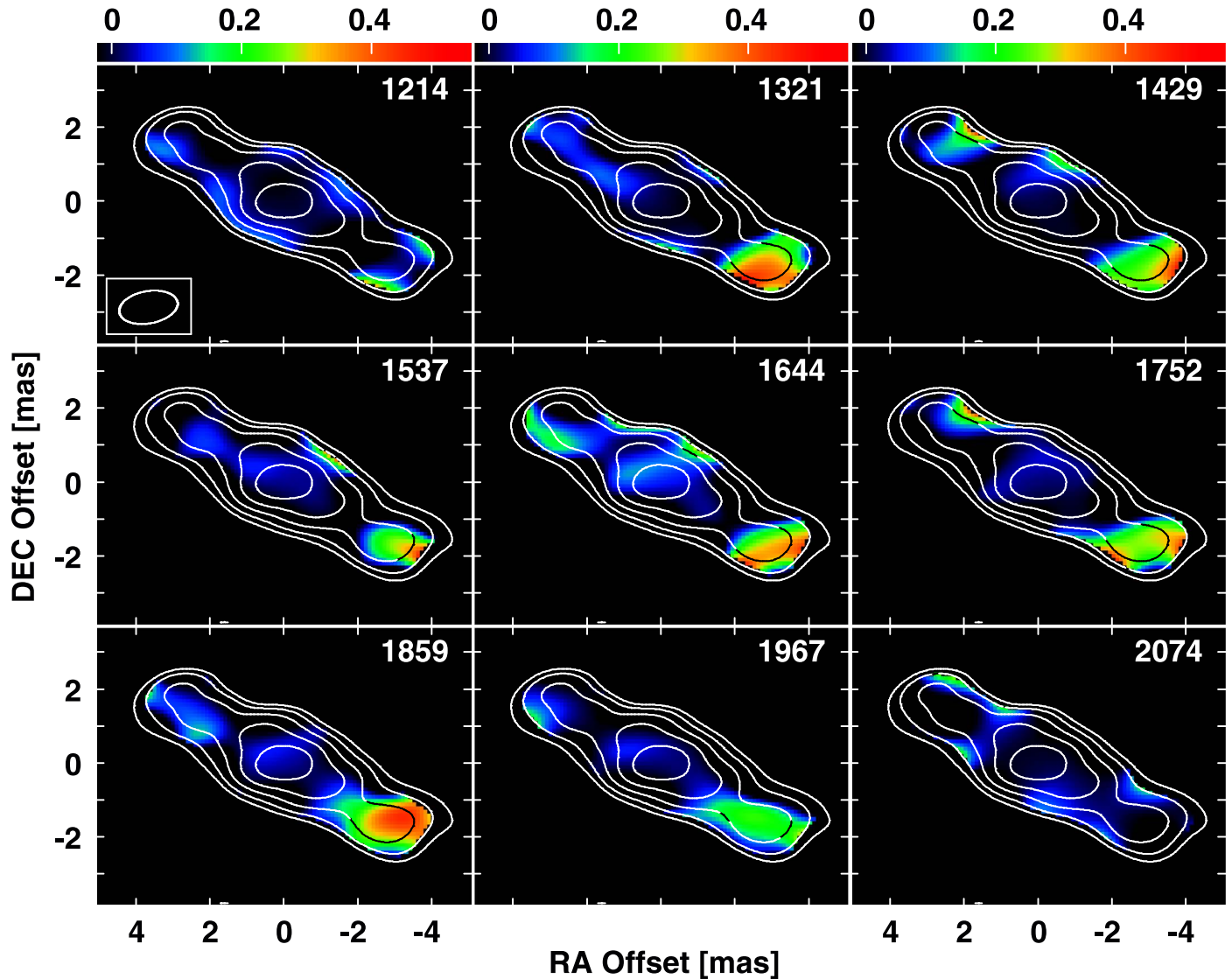


**Figure 3.** Color channel maps of the  $\text{HCO}^+(1-0)$  optical depth averaging every 32 MHz ( $108 \text{ km s}^{-1}$ ), overlaid by a contour map of  $\lambda 3 \text{ mm}$  continuum emission (Figure 2(f)). Color indicates the optical depth of  $\text{HCO}^+$  absorption. Their central velocities are shown at the upper right. The rms noise in optical depth is 0.02 and 0.09 on the central and western receding jet components, respectively.

angular resolution. It is one order higher than that obtained from the PdBI observations (Liszt & Lucas 2004). This fact suggests that the  $\text{HCO}^+$  covering factor is much larger on subparsec scales. Here we examine it by estimating the mean opacity over the whole  $\sim 0.7 \text{ pc}$  nuclear structure for each frequency channel  $\langle \tau_\nu \rangle$ , using

$$\langle \tau_\nu \rangle = \frac{\iint \tau_\nu(x, y) I(x, y) dx dy}{\iint I(x, y) dx dy}, \quad (1)$$

where  $\tau_\nu(x, y)$  is the  $\text{HCO}^+$  opacity distribution for each channel map (color map in Figure 3), and  $I(x, y)$  is the  $\lambda 3 \text{ mm}$  continuum image (Figure 2(f)). We also calculated normalized flux density for each channel from  $\langle \tau_\nu \rangle$ , and listed it in Table 1. The derived normalized flux density is in the range from 0.96 to 1, and it is in good agreement with the  $\text{HCO}^+$  absorption profile on hundred-parsec scales observed with the PdBI (Liszt & Lucas 2004). Thus, the  $\text{HCO}^+$  covering factor varies on

Central Velocity ( $\text{km s}^{-1}$ ) (1)	$\langle \tau_\nu \rangle$ (2)	Normalized Flux Density (3)
1214	0.0014	0.999
1321	0.0191	0.981
1429	0.0165	0.984
1537	0.0038	0.996
1644	0.0384	0.962
1752	0.0198	0.980
1859	0.0400	0.961
1967	0.0137	0.986
2074	0.0040	0.996

**Note.** (1) Central velocity for each channel; (2) mean opacity over the whole parsec-scale nuclear source; (3) normalized flux density calculated from the values in (2).

scales in the center of NGC 1052, and the difference in HCO<sup>+</sup> optical depth between KVN and PdBI could account for the partial covering of HCO<sup>+</sup> absorbing gas on subparsec scales.

Concentration of high HCO<sup>+</sup> opacity on the western receding jet component strongly suggests that HCO<sup>+</sup> absorption is associated with the parsec-scale circumnuclear torus. Because the jet axis of NGC 1052 is oriented within  $\sim 30^\circ$  from the sky plane (e.g., Kellermann et al. 1999; Kamenno et al. 2001; Kadler et al. 2004b), the near side of the thick torus should lie in front of the nuclear component and the receding jet component. The line of sight to the receding jet passes through the near side of the torus, where the HCO<sup>+</sup> absorption occurs. The HCO<sup>+</sup> gas presents a relatively common distribution with plasma, H<sub>2</sub>O, OH, and HCN. If the torus has several physical layers as shown in Figure 3 of Sawada-Satoh et al. (2016), the HCO<sup>+</sup> gas could be located in the cooler ( $< 400$  K) molecular layer inside the torus, where the HCN gas also could lie.

We can estimate the total column density of HCO<sup>+</sup> assuming the local thermodynamic equilibrium, using the approximate expression for the  $J = 1-0$  transition

$$N_{\text{tot}} = \frac{3k(T_{\text{ex}} + hB/3k)}{8\pi^3 B \mu^2 [1 - \exp(-h\nu/kT_{\text{ex}})]} \int \tau d\nu, \quad (2)$$

where  $k$  is the Boltzmann constant,  $h$  is the Planck constant,  $\mu$  is the permanent dipole moment of the molecule,  $B$  is the rotational constant,  $T_{\text{ex}}$  is the excitation temperature, and  $\int \tau d\nu$  is the velocity-integrated optical depth of the absorption feature. For HCO<sup>+</sup>,  $\mu$  is 4.07 Debye (Haese & Woods 1979) and  $B = 44,594$  MHz (Lattanzi et al. 2007). As  $T_{\text{ex}}$  is uncertain, here we assume  $T_{\text{ex}} = 100$  and 230 K, in the same manner as Sawada-Satoh et al. (2016). Assuming  $\int \tau d\nu = \tau_p \Delta\nu$  for the peak absorption channel at 1658 km s<sup>-1</sup>, the total column density of HCO<sup>+</sup> of the peak is calculated to be  $(1.5 \pm 0.3) \times 10^{15}$  cm<sup>-2</sup> and  $(7.6 \pm 1.5) \times 10^{15}$  cm<sup>-2</sup> at 100 and 230 K, respectively. The column density ratio between HCN and HCO<sup>+</sup> around 1658 km s<sup>-1</sup> can be determined to be  $\sim 6.5$ , as the total HCN column density at 1656 km s<sup>-1</sup> is  $9.5 \times 10^{15}$  cm<sup>-2</sup> and  $5.0 \times 10^{16}$  cm<sup>-2</sup> at 100 and 230 K, respectively (Sawada-Satoh et al. 2016). The derived value of the column density ratio is even higher compared to the high HCN/HCO<sup>+</sup> intensity ratios ( $R_{\text{HCN}/\text{HCO}^+} \sim 2$ ) measured in NGC 1097 (Izumi et al. 2013) and NGC 1068 (García-Burillo et al. 2014; Viti et al. 2014) on parsec scales with the Atacama Large Millimeter/submillimeter Array (ALMA). However, we have to note that the column densities of HCN and HCO<sup>+</sup> are not measured simultaneously. During a time gap of 27 months between the two observations of HCN and HCO<sup>+</sup>, the background receding jet component could move 0.18 pc outward, almost one beam size. Adopting an abundance ratio HCO<sup>+</sup> relative to H<sub>2</sub> of  $(2-3) \times 10^{-9}$  in Galactic diffuse molecular gas (Liszt & Lucas 2000, 2004; Liszt et al. 2010), the column density of molecular hydrogen (H<sub>2</sub>) is derived to be  $N_{\text{H}_2} \sim 10^{24-25}$  cm<sup>-2</sup>, which is consistent with  $N_{\text{H}_2}$  estimated from the HCN absorption spectrum (Sawada-Satoh et al. 2016).

Despite the detection of HCO<sup>+</sup> (1-0) absorption, the emission of HCO<sup>+</sup> has not been found in the center of NGC 1052 with the past PdBI observation (Liszt & Lucas 2004). This indicates that the H<sub>2</sub> volume density ( $n_{\text{H}_2}$ )

in the center is less than the H<sub>2</sub> critical density ( $n_{\text{cr}}$ ) for HCO<sup>+</sup> (1-0) emission. Adopting the Einstein coefficient for spontaneous emission  $A_{10} = 4.52 \times 10^{-5}$  s<sup>-1</sup> for HCO<sup>+</sup> (Izumi et al. 2013), and the collisional rate  $\gamma_{10}$  of  $1.8 \times 10^{-10}$  cm<sup>-3</sup> s<sup>-1</sup> at a temperature of 100 K (Flower 1999), gives a critical density  $n_{\text{cr}} = A_{10}/\gamma_{10}$  of approximately  $2.5 \times 10^5$  cm<sup>-3</sup>. Thus, it derives  $n_{\text{H}_2} < 2.5 \times 10^5$  cm<sup>-3</sup>. The relation  $N_{\text{H}_2} = n_{\text{H}_2} f_v L$ , where  $f_v$  is the volume-filling factor and  $L$  is the size of the molecular gas region in the torus, gives a lower limit  $L > 1/f_v$  pc, using  $N_{\text{H}_2} = 10^{24}$  cm<sup>-2</sup> and  $n_{\text{H}_2} < 2.5 \times 10^5$  cm<sup>-3</sup> at 100 K. If we assume that the molecular region is inhomogeneous (i.e.,  $f_v < 1$ ),  $L$  would be even larger than 1 pc.

It is remarkable that a broad HCO<sup>+</sup> absorption with a redshifted peak and a blueshifted wing is detected against the parsec-scale receding jet of NGC 1052. The broad spectral profile is much wider than expected from the thermal broadening ( $\sim 0.2$  km s<sup>-1</sup>), and it suggests a significant contribution of other kinematics, or a complex combination of some rapid motion with multiple clumpy gas clouds at various different velocities, such as turbulence, interaction, and so on. The spectral profile was not resolved into several narrow absorption features. However, the optical depth differential among different velocity channel maps implies that several gas clumps or inhomogeneous structure at various velocities lie along the line of sight and apparently overlap. It is likely that the redshifted HCO<sup>+</sup> absorption around the peak velocity trace the same infall motion as HCN absorption and H<sub>2</sub>O maser inside the torus. It can be interpreted as infall toward the supermassive black hole of NGC 1052. In addition to the infall motion, the blueshifted HCO<sup>+</sup> absorbing gas could indicate small-scale turbulence of clumps inside the torus.

## 5. Summary

Our 1 mas angular resolution observations toward the center of NGC 1052 with the KVN have led us to first subparsec-scale imaging of the HCO<sup>+</sup> absorbing gas in the vicinity of AGN. The spectral profile of HCO<sup>+</sup> absorption is detected in a broad velocity range of 1350–1850 km s<sup>-1</sup>, in agreement with the past PdBI observations. However, the peak absorption depth is deeper than that of the PdBI. Our HCO<sup>+</sup> optical channel map clearly shows a high opacity on the receding jet component, and a faint opacity on the nuclear component. It suggests that HCO<sup>+</sup> absorption arises from the near side of the torus, which covers the receding jet and the nucleus. We estimate  $N_{\text{H}_2}$  of  $10^{24-25}$  cm<sup>-2</sup>, assuming an abundance ratio [HCO<sup>+</sup>]/[H<sub>2</sub>] of  $(2-3) \times 10^{-9}$  and a  $T_{\text{ex}}$  of 100–230 K. Because HCO<sup>+</sup> line appears only in absorption even with the PdBI, we find  $n_{\text{H}_2} < n_{\text{cr}} = 2.5 \times 10^5$  cm<sup>-3</sup>. It implies that the radius of the torus is  $> 1$  pc. The HCO<sup>+</sup> absorbing is probably several gas clumps with several different velocities, rather than a single uniform medium with a single velocity. The broad HCO<sup>+</sup> absorption could consist of several kinematics at various velocities inside the torus.

We are grateful to all members of KVN for supporting our observations. The KVN and a high-performance computing cluster are facilities operated by the KASI (Korea Astronomy and Space Science Institute). The KVN observations and correlations are supported through the high-speed network connections among the KVN sites provided by the KREONET (Korea Research Environment Open NETWORK), which is managed and operated by the KISTI (Korea Institute of

Science and Technology Information). S.K. was supported by JSPS KAKENHI grant No. JP18K03712. S.S.L. was supported by the National Research Foundation of Korea (NRF) grant funded by the Korea government (MSIP; NRF-2016R1C1B2006697).

Facility: KVN.

### ORCID iDs

Satoko Sawada-Satoh  <https://orcid.org/0000-0001-7719-274X>

Do-Young Byun  <https://orcid.org/0000-0003-1157-4109>

Sang-Sung Lee  <https://orcid.org/0000-0002-6269-594X>

Seiji Kameno  <https://orcid.org/0000-0002-5158-0063>

### References

- Braatz, J. A., Wilson, A. S., & Henkel, C. 1994, *ApJL*, 437, L99
- Deller, A. T., Tingay, S. J., Bailes, M., & West, C. 2007, *PASP*, 119, 318
- Flower, D. R. 1999, *MNRAS*, 305, 651
- García-Burillo, S., Combes, F., Usero, A., et al. 2014, *A&A*, 567, A125
- Greisen, E. W. 2003, in *Information Handling in Astronomy—Historical Vistas*, Vol. 285, ed. A. Heck (Dordrecht: Kluwer), 109
- Guainazzi, M., & Antonelli, L. A. 1999, *MNRAS*, 304, L15
- Haese, N. N., & Woods, R. C. 1979, *CPL*, 61, 396
- Han, S.-T., Lee, J.-W., Kang, J., et al. 2008, *IJIMW*, 29, 69
- Han, S.-T., Lee, J.-W., Kang, J., et al. 2013, *PASP*, 125, 539
- Impellizzeri, V., Roy, A. L., & Henkel, C. 2008, *PoS*, 2008, 33
- Izumi, T., Kohno, K., Martín, S., et al. 2013, *PASJ*, 65, 100
- Jensen, J. B., Tonry, J. L., Barris, B. J., et al. 2003, *ApJ*, 583, 712
- Jones, D. L., Wrobel, J. M., & Shaffer, D. B. 1984, *ApJ*, 276, 480
- Kadler, M., Kerp, J., Ros, E., et al. 2004a, *A&A*, 420, 467
- Kadler, M., Ros, E., Lobanov, A. P., Falcke, H., & Zensus, J. A. 2004b, *A&A*, 426, 481
- Kameno, S., Inoue, M., Wajima, K., Sawada-Satoh, S., & Shen, Z.-Q. 2003, *PASA*, 20, 134
- Kameno, S., Nakai, N., Sawada-Satoh, S., Sato, N., & Haba, A. 2005, *ApJ*, 620, 145
- Kameno, S., Sawada-Satoh, S., Inoue, M., Shen, Z.-Q., & Wajima, K. 2001, *PASJ*, 53, 169
- Kellermann, K. I., Vermeulen, R. C., Cohen, M. H., & Zensus, J. A. 1999, *BAAS*, 31, 20.02
- Kellermann, K. I., Vermeulen, R. C., Zensus, J. A., & Cohen, M. H. 1998, *AJ*, 115, 1295
- Lattanzi, V., Walters, A., Drouin, B. J., & Pearson, J. C. 2007, *ApJ*, 662, 771
- Lee, S.-S., Byun, D.-Y., Oh, C. S., et al. 2015b, *JKAS*, 48, 229
- Lee, S.-S., Oh, C. S., Roh, D.-G., et al. 2015a, *JKAS*, 48, 125
- Liszt, H., & Lucas, R. 2000, *A&A*, 355, 333
- Liszt, H., & Lucas, R. 2004, *A&A*, 428, 445
- Liszt, H. S., Pety, J., & Lucas, R. 2010, *A&A*, 518, A45
- Middelberg, E., Roy, A. L., Walker, R. C., & Falcke, H. 2005, *A&A*, 433, 897
- Oh, S.-J., Roh, D.-G., Wajima, K., et al. 2011, *PASJ*, 63, 1229
- Omar, A., Anantharamaiah, K. R., Rupen, M., & Rigby, J. 2002, *A&A*, 381, L29
- Rioja, M., & Dodson, R. 2011, *AJ*, 141, 114
- Sawada-Satoh, S., Kameno, S., Nakamura, K., et al. 2008, *ApJ*, 680, 191
- Sawada-Satoh, S., Roh, D.-G., Oh, S.-J., et al. 2016, *ApJL*, 830, L3
- Ulich, B. L., & Haas, R. W. 1976, *ApJS*, 30, 247
- van Gorkom, J. H., Knapp, G. R., Raimond, E., Faber, S. M., & Gallagher, J. S. 1986, *AJ*, 91, 791
- Vermeulen, R. C., Ros, E., Kellermann, K. I., et al. 2003, *A&A*, 401, 113
- Viti, S., García-Burillo, S., Fuente, A., et al. 2014, *A&A*, 570, A28
- Weaver, K. A., Wilson, A. S., Henkel, C., & Braatz, J. A. 1999, *ApJ*, 520, 130
- Wrobel, J. M. 1984, *ApJ*, 284, 531
- Yeom, J. H., Oh, S. J., Roh, D. G., et al. 2009, *JASS*, 26, 567